

CrystEngComm

Accepted Manuscript



This is an *Accepted Manuscript*, which has been through the Royal Society of Chemistry peer review process and has been accepted for publication.

Accepted Manuscripts are published online shortly after acceptance, before technical editing, formatting and proof reading. Using this free service, authors can make their results available to the community, in citable form, before we publish the edited article. We will replace this *Accepted Manuscript* with the edited and formatted *Advance Article* as soon as it is available.

You can find more information about *Accepted Manuscripts* in the [Information for Authors](#).

Please note that technical editing may introduce minor changes to the text and/or graphics, which may alter content. The journal's standard [Terms & Conditions](#) and the [Ethical guidelines](#) still apply. In no event shall the Royal Society of Chemistry be held responsible for any errors or omissions in this *Accepted Manuscript* or any consequences arising from the use of any information it contains.

Influence of Oleic Acid on the Nucleation and Growth of 4-N, N-dimethylamino-4-N-methyl-stilbazoliumtosylate (DAST) crystals

Tina Thomas^a, Jerald V. Ramaclus^{b*}, Fausto P. Mena^b, Edgar Mosquera^c, P. Sagayaraj^a and Ernest A. Michael^b

^a Department of Physics, Loyola College, Chennai, India - 600034.

^b Department of Electrical Engineering, University of Chile, Av. Tupper 2007, Santiago, Chile -8370451. Email: jerald.ramaclus@raig.uchile.cl, jeraldramaclus@gmail.com

^c Department of Materials Science, University of Chile, Av. Tupper 2069, Santiago, Chile-8370451.

A simple method to control the nucleation and morphology of (4-N, N-dimethylamino-4-N-methyl-stilbazoliumtosylate) DAST crystals is explored. At equal concentration of oleic acid and DAST in methanol, pure DAST crystals with an irregular hexagonal shape are obtained by solvent evaporation method. The influence of oleic acid on facilitating growth in specific faces is investigated. The purity of the grown crystal is investigated by Powder XRD, NMR and Raman spectroscopy analyses. As a major improvement we present a method where a preference in the growth of one of the desired faces (010) in the final morphology of the DAST crystal is possible which would be attractive for Terahertz generation and detection studies.

Introduction

Development of technology for the terahertz (THz) spectral range (also known as the submillimeter or far-infrared range) is an extremely attractive research field, with interest from sectors as diverse as space and atmospheric sciences, spectroscopy and astronomy, semiconductors and microelectronics, defense and home security, medical and pharmaceutical, manufacturing and material science, as well as agriculture and forensic science¹. In particular, astronomy and space research have been two of the strongest drivers for THz research and, as a consequence, international projects like the Atacama Large Millimeter/sub-millimeter Array (ALMA) are already operating in Chile. ALMA is considered to be one of the world's largest astronomical project². Moreover, in 2004, the Massachusetts Institute of Technology, MIT, classified THz technology as one of the ten new technologies that is going to change our lives³.

There is a vast array of potential sources of THz waves each with relative advantages, and advances in various research areas continue to provide new candidates⁴. However, high emission power at a low cost for a portable room temperature THz source are the major constraints for future THz systems, which is difficult to achieve due to the fact that the power levels of present electronic and optical devices decrease rapidly as they approach the range of 1 to 10 THz, the so-called "terahertz gap"¹. Among the two techniques which are efficient in this frequency region, p-Ge laser require cryogenic temperatures for continuous-wave operation which raises the cost as well as the size of the equipment. The other is difference frequency generation (DFG) by a nonlinear optical crystal is advantageous due to room temperature operation and to even a broader THz output spectrum as produced by the widely used ultrafast photoconductive devices^{5, 6}. This suggests that the nonlinear optical (NLO) method is a potential technique for THz generation.

Materials that find attention in this field can be broadly classified into three categories, Semiconductors, Inorganic electro-optic crystals and Organic electro optic crystals. LiNbO₃ and LiTaO₃ are inorganic crystals having low nonlinear optical (NLO) coefficients with their high dielectric constant making them less popular⁷. ZnTe, GaP, GaAs, GaSe, CdTe and InP are some of the semiconductor materials which possess large NLO coefficients compared to inorganic crystals. However, most of these materials are cubic crystals and hence, the birefringence effect is absent for phase matching which reduces the performance of difference frequency generation sources. The NLO coefficient and phase matching ability are the defining factors that determine the conversion efficiency in difference frequency generation or nonlinear optical process in general⁸.

In this scenario, dominated by semiconductors, an organic crystal DAST, have attracted much attention due to its very high NLO coefficients namely, $d_{111}=1230$ pm/V, $d_{311}=239$ pm/V, $d_{122}=166$ pm/V, and $d_{212}=d_{221}=135$ pm/V at 800 nm. At the same time, it has a low dielectric constant making it highly suitable for THz generation⁹. In many cases, the tuning range of THz waves generated by inorganic NLO material is limited by the material characteristics. Then, coverage of a wide frequency range requires different source systems. On the other hand, the use of an organic NLO crystal introduces the feasibility of ultra wide tunability due to the presence of large anisotropy and birefringence^{10, 11}. Recently ultra-broad band pulsed terahertz generation using a DAST crystal up to 200 THz has also been demonstrated where the high-frequency components beyond 100 THz are much stronger than conventional electro-optic crystals such as GaSe¹².

Though DAST is considered as one of the best THz emitters, its development is limited by its crystal growth characteristics. DAST has a high tendency to form multi-nucleation leading to poly-crystallization and twinning which at the same time reduces the quality and size of the single crystals^{13, 14}. Under humid conditions hydrated co-crystals with centrosymmetric structure are grown preventing solvent evaporation (SE) method, which is the simplest method for crystal growth¹⁵. Most importantly, the final morphology of the DAST crystal when grown from methanol does not exhibit the desired faces required for efficient THz generation¹⁶. The d_{111} and d_{122} are the preferred largest NLO coefficients and in order to exploit those, the (100) and (010) faces are required to be aligned toward the optical axis, respectively^{17, 18}. However, DAST grows as a crystal from the pure methanol

solution without the (100) and (010) faces¹⁹. Therefore, DAST crystals are mechanically modified by cutting, polishing and other sophisticated techniques to obtain the required morphology during which, however, a lot of the expensive purified starting substance of the growth is lost.²⁰⁻²²

In this article we propose a simple cost-effective method which allows to grow the pure DAST crystals by SE method directly with the desired morphology required for efficient THz-generation. Additionally, it has the welcomed side-effect to reduce multi-nucleation. This is achieved using additives (crystal growth modifiers). Researchers have used additives to control the nucleation and morphology of DAST before but no significant work has been reported yet that modifies or develops a face other than the usual (100), (110), (-110), (-1-10) and (1-10) faces in bulk crystal form²³⁻²⁸. All these reports have been demonstrated using slow-cooling method due to the issue of hydration during growth by SE method. Hence, the influence of additives in DAST crystal growth by SE method remains unclear. The choice of a suitable additive for SE method to grow DAST crystal is of significant importance as it should have the ability to prevent hydration and also lead to the desired morphology. Oleic acid (OA) has been used as an additive to control the nucleation in several inorganic crystals due to its superior inhibiting, stabilizing and adsorption properties.^{29, 30} The presence of a long alkyl chain and an unsaturated double bond provide significant hydrophobicity to the material that adsorbs it; this property is particularly attractive to prevent hydrated DAST crystallization.³¹ Therefore, due to its attractive properties as a crystal growth modifier, in this article, we have investigated the influence of OA on the control of the nucleation, growth and morphology of the DAST crystals by SE method.

Experimental

Nucleation Studies

The nucleation point of DAST in methanol with OA was measured as follows. A volume of 5 ml of saturated solution of DAST in methanol at 20 °C was taken in a test tube and the solvent was allowed to evaporate. At the point where the first nucleation occurs, the quantity of the remaining solvent was measured and its equilibrium concentration was calculated based on the solubility curve. This process was repeated at 25 and 30 °C for three different mole ratios of DAST (MW=410.62 g/mol) and oleic acid (MW=282.46 g/mol) in methanol; 1:0 (sample A), 1:1 (sample B) and 1:2 (sample C). The nucleation mechanism was further investigated by casting a drop of DAST-OA-methanol solution of three different compositions mentioned earlier on a glass slide at 25 °C. The nucleation was recorded using a CCD sensor through an optical microscope.

Crystal Growth

DAST crystals were grown by the spontaneous nucleation, SE method in the absence and presence of OA as an additive. Three different solutions of DAST-methanol and OA (according the compositions used in nucleation studies) were prepared, each in a 16 ml of methanol at 20 °C (Table 1 of supplementary information). The measured quantities of DAST were first dissolved in methanol by heating and then transferred to 18 ml plastic test tubes. The solutions were allowed to cool and later the measured quantities of OA were added to each test tube, sealed and allowed to disperse through mechanical shaking for 5 hours. Then the test tubes were kept in a constant temperature bath at 21 °C for 1 day. After one day no separation of OA was observed and it was found visually to be dispersed well in the solution. The temperature was reduced to 20 °C and the seals of the test tubes were replaced by perforated lids. In this way the solvent was allowed to evaporate at a rate of 0.8 ml per day.

Characterization

The nucleation mechanism and etching analyses were studied by using an Olympus-BX41-LED optical microscope. Powder X-ray diffraction analysis was performed using a Siemens P4 diffractometer in order to identify the structure. The morphology of the single crystals was investigated by using a Bruker D8 Quest single crystal X-ray diffractometer equipped with a photon 100 CMOS detector. The morphology of the DAST crystal was simulated using WinXMorph software by updating the lattice parameters and symmetry system of DAST.³² The angle between the planes were calculated using the “calculate angle” option and by choosing the planes. The angle of the single crystal faces were also measured using a contact goniometer. The proton NMR spectrum was recorded using Bruker Avance III 500 MHz FT NMR spectrometer with deuterated methanol as the solvent. Raman Spectra were measured using Bruker RFS 27 standalone FT-Raman spectrometer in the spectral range of 50 - 4000 cm⁻¹ with a Nd:YAG laser source at 1064 nm.

Results and discussion

Nucleation

It was observed that the rate of nucleation increased from sample C to sample A (Fig. 1). Hence, the metastable zone width is largest in the sample C and decreased toward A. It has been reported that additives suppress the cluster formation and increase the metastable zone width resulting in fewer but larger crystals with higher quality.²⁹ The large metastable zone width due to the presence of OA, when compared to other additives used previously, is expected to result in larger crystals than in previous works.²³⁻²⁵ The excess OA (more than equal ratio of DAST in samples C) has increased the critical size of the nucleus and hence crystal growth could not proceed until the nucleus reached the enhanced critical activation energy to overcome the inhibiting process. Only those nuclei which overcame the critical energy have grown into crystals and others have dissolved and transported to the growing crystal due to concentration gradients. Therefore, OA has significantly affected the nucleation.

Spherulites were observed when the nucleation mechanism was investigated on the glass slides and these studies provide more insights on the nucleation behavior of DAST in different compositions of OA in methanol. In sample A, primary and secondary nucleation could also be observed in form of spherulites and a concentration gradient around the existing crystal respectively (movie 1). When these spherulites are viewed between crossed polarization filters, they produce the Maltese extinction cross (Fig 2a and b) which vindicates that these are not polycrystalline aggregates.³³ It can be observed that the primary nucleation accompanies the cluster formation first and once the critical size is achieved they grow as a crystal. These clusters, which are highly disordered, are the origin of spherulite formation.³⁴ Once the crystal forms, the spherulite disappears because of the diminishing disorder due to the crystalline nature.

A similar mechanism like that of sample A is observed in sample B where the cluster formation and subsequent growth into crystals takes place (Movie 2). The major difference here is the pattern of the noncrystallographic branching which is a consequence of the change in characteristics of the cluster; the existence of a smaller cluster and appearance of partial crystalline core which exists inside the cluster (Fig. 2 c and d). OA has disconnected most of the spherulites from the neighboring ones unlike in sample A where the spherulites were connected via the branches; this suggest that the transport of solute to the nucleus has been affected.³⁵

In case of sample C, the nuclei are completely separated by OA and the branching from the nucleus is not as uniform as sample A or B (Fig. 2. e and f). It appears that in this case the spherulite adopted a different branching growth mechanism (Movie 3). The formation of crystals inside the cluster suggest the possibility of a two-step nucleation mechanism inside the core of the spherulite (Fig. 2f).³⁶ The secondary nucleation via concentration gradient is also completely affected by the OA which surrounds it. The emergence of the crystal inside the cluster completely eliminates the noncrystallographic branching around the core. The suppression of cluster formation by OA is evident from the relationship between the cluster and the noncrystallographic branching associated with the spherulite observed in samples A, B and C. It is to be noted that in sample A, polycrystals appear and the samples B and C are free from such polycrystals during the nucleation studies. The longer time that samples B and C take to nucleate was recorded in videos and the observation of suppression of cluster formation further supports the increase of the metastable zone width. This strongly suggests that OA efficiently affects the way the DAST is nucleating. The phenomenon observed on a glass plate cannot be suggested as the nucleation mechanism inside the solution of the growing crystal, but can be used as an indication for possible changes in the morphology due to the influence of OA on nucleation of DAST.

Single Crystal Characteristics

The major consequences of nucleation control and large metastable zone is the size enhancement of the crystal and morphology changes. After 20 days of growth, crystals of different sizes were obtained. At the end of the growth, when all methanol evaporated, OA was settled at the bottom of the crystals and was also sticking to the crystals. In sample B most of the crystals appeared to be twinned or polycrystals but in fact they were sticking together due to OA and could be easily separated. In appearance, samples A and C are reddish in color and also transparent, whereas sample B is with metallic green luster and not transparent (Fig. 3). In sample C, the largest single crystal harvested was of the size of $25 \times 5 \times 0.5 \text{ mm}^3$ as shown in Figure 3c. It can be observed that the OA is an effective additive to control nucleation and growth of DAST crystals. As the proportion of OA increases with respect to DAST, the bigger crystals were obtained which directly reflects the consequence of a wider metastable zone.

Another important issue in growing DAST crystals by evaporation method is the formation of hydrated co-crystals and in order to investigate this, powder XRD was performed on the 001 face of the grown crystals of all samples (Fig 4). For comparison we have also measured the powder XRD of the finely powdered pure DAST which was annealed at 100°C for 1 hour to remove any water molecule that might be present. From the simulated powder XRD of hydrated DAST we observe that some of the peaks coincide with pure DAST especially at 12° and 24° (Fig. S1). The major difference is, a peak observed at 6° in case of hydrated DAST and absent in pure DAST. Since most of the earlier research works reported the powder XRD patterns of DAST in the range of 10 to 40° the possibility of hydration is overlooked in case of SE methods^{23,27,28,37,38}. Therefore, in order to distinguish between pure and hydrated DAST, the powder XRD has to be measured from 5° where a peak around 6° is observed only in the hydrated-DAST (Triclinic Pt) and not in the pure DAST (monoclinic Cc). In case of sample A, the major peaks at 6.1° , 12.2° and 24.6° corresponds to (001), (002) and (004) planes of the Triclinic Pt (Fig. 4a and Fig S1) and not the monoclinic Cc crystal system (Fig 4d)¹⁵. Sample B is found to be in good agreement with the powder XRD pattern of pure DAST and the peak around 6° is absent (Fig. 4b). Usually, DAST crystals grown from evaporation method form hydrated co-crystals and here, the hydrophobicity of OA could have prevented such formation¹⁵. The powder XRD pattern of sample C possess the characters of both forms of DAST (Fig 4c). We can observe the peaks at 6.1 , 12.2 and 24.6 however with lower intensity with respect to those of pure DAST. It could be possible that the crystal is partially hydrated; the outer layers of the DAST crystal are hydrated. Further, in order to determine if OA is present as an impurity in sample B, NMR and Raman spectra were measured. In the NMR analysis, there were no major peaks other than DAST was observed (Fig. S2, S3 and S4)^{39,40}. Oleic acid has major peaks at 5.35 , 1.45 to 1.23 due to $\text{HC}=\text{CH}$, $(\text{CH}_2)_3$ and $(\text{CH}_2)_5$ Hydrogens respectively and there is no trace of such peaks in the sample B. In case of Raman spectrum of sample B, the peaks match perfectly with those of pure DAST. There are negligible shift in the peaks which may due to unknown experimental conditions. Oleic acid possesses a very strong Raman peak around 2800 cm^{-1} and its absence clearly indicates that sample B is free of oleic acid⁴¹.

Crystal Growth and Morphology

The morphology of DAST crystals is significantly affected by the influence of OA in case of sample B. Growth conditions like evaporation rate and concentration also strongly affects the shape of a crystal and in case of DAST such conditions produce either thicker or thinner crystals^{42,43}. In another method mixed solvent were used to control the thickness of the crystals which

demonstrates the anisotropic growth of DAST in a preferred direction due to the interaction of different solvents⁴³. Usually DAST crystals grow along the a-b plane in slow-cooling method thus having square platelet morphology with the (001) face as the large surface area. The other faces that show up in the final morphology are the (110), (1-10), (-110) and (-1-10).¹⁶ Square shaped DAST crystals are also obtained by evaporation method but mostly they turn out to be hydrated. In few cases, hexagonal shaped DAST crystals were observed at high supersaturations as microcrystals or twinned bulk crystals (by temperature lowering and SE methods)^{44,45}. It is reported that the growth rates of (100) and (010) planes were almost similar and during prolonged growth the (020) face finally disappears in bulk crystals.⁴⁴ In the present work, in the case of sample B, we find that crystals form in irregular hexagonal shape (Fig 3d) with the (010) face emerging and existing in the final morphology at a supersaturation temperature of 20 °C. This is an indication of the influence of OA on DAST crystal growth. It has been reported that twinned crystals possess a flat surface with (001) face on both the sides and these crystals are in irregular hexagon shape.⁴⁵ In order to identify the faces of the largest surface of the DAST crystals grown from sample B, one crystal was subjected to single-crystal X-ray diffraction analysis. The unit cell parameters were obtained as follows; $a = 10.3652(5) \text{ \AA}$, $b = 11.3225(2) \text{ \AA}$, $c = 17.8937(1) \text{ \AA}$, $\beta = 92.242(2)^\circ$ and $V = 2100.00(4) \text{ (\AA}^3\text{)}$ with monoclinic Cc space group, which is in good agreement with the literature.¹⁹ Once the unit cell parameters and orientation matrix were obtained, face indexing was performed which revealed that one of the flat surfaces is (001) and the other (00 $\bar{1}$) (Fig.S5). This confirms that the crystals are not twinned and the hexagonal shape is not a consequence of twinning. Therefore, we find that, this change in shape is not due to the factors as observed in the earlier literature.

The existence of the (010) face in the grown crystal was further confirmed by measuring the interfacial angle between the planes by a contact goniometer. The measured angles of 95° between the (1 $\bar{1}$ 0) and (110) faces and 135° between the (1 $\bar{1}$ 0) and (010) faces are found to be close to the values simulated for the DAST crystal system (95.1° and 135.45°) (Fig. 5). It was found that the (010) face did not grow completely in sample B. This incomplete growth of the crystal is attributed to the depletion of solute at the end of the growth (Fig. 3d). When the surface of sample B was etched with methanol for 10 s, it revealed the 2-dimensional growth mechanism which is hexagonal with (010) as a major face (Fig. 6a and 6b). In order to confirm that it is OA that is responsible for such pattern we also used the composition of OA in methanol according to sample B and etched the surface of pure DAST crystal grown from methanol. The etch patterns are leading to hexagon is evident from Figure 6c. When a similar pure DAST crystal was etched with methanol (no OA) for the same duration we did not observe a hexagonal etch pattern (Fig. 6b) but instead a typical pattern (Fig. 6d) as reported earlier for DAST²⁵. Therefore, it becomes evident that it is OA which inhibits the growth on the (010) direction directly through the interaction with DAST.

The possible roles of OA in the DAST methanol solution are (i) as a dimer due to hydrogen bonding interaction with the solvent, (ii) de-protonation of OA due to the ionic nature of DAST and (iii) interaction of hydrogen bonding with the anion of the DAST. It has been reported that, when OA is used as an additive in a polar solvent, it has the tendency to form dimers due to hydrogen bonding interaction with the solvent.⁴⁶ Apart from that, the carboxyl hydrogen atom of the oleic acid could also form bonding with the hydroxyl group of the methanol.⁴⁷ Therefore, these reports suggest that the hydroxyl group of the OA has a strong tendency to form a hydrogen bond with any molecule. If OA would have deprotonated, it would have affected, when attached to the crystal the Van der Waals forces and hydrogen bonds between the cations and that of the anions resulting in a hindrance along the a-axis. However, the (100) has not emerged which reveals that deprotonation did not occur and also, since OA is not an ionic molecule, it is highly unlikely. The observation from the spherulite growth reveals that the OA has affected the branching; OA has inhibited the interaction of methanol with DAST molecules. Since methanol molecules are involved in the dissolution of DAST ions, they are less likely to form hydrogen bonding with OA. The emergence of the (010) face clearly vindicates the interaction of hydroxyl group of OA and oxygen of the DAST anions, as the (010) surface exposes these oxygen atoms to the solution and the OA, resulting in an inhibited growth along the b-axis.

It is known that the hydrogen bondings between the oxygens of the tosylate anions and the hydrogens of the olefin- and benzene-parts play a vital role in packing the DAST molecules in parallel alignment and stacking them along the b-axis. Follonier et al. reported that adjacent cation molecules are bound by Van der Waals forces between the donor of one molecule, and the acceptor of the next-lying molecule, which is responsible for the growth along the a-axis.⁴⁸ The strongest hydrogen bonds (2.636 Å) between two adjacent tosylates in the DAST crystal along the b-axis are a major binding force to grow along that direction (Fig. S6). The other strong hydrogen bonds between the CH— atoms of the cations and —OS groups of anions with distances of alternately 2.615 and 2.454 Å are responsible for the parallel alignment of the cation molecules. It is evident from the structure that the hydrogen bonds between the anions are also responsible for the growth along the b-axis and OA has interacted with this hydrogen bonding so that the growth along the b axis is hindered (Fig. 7). We can summarize these findings as follow. (i) When there is no OA, the DAST grows along the a- and b-axes at the same rate; (ii) when OA is present at an equal ratio to that of DAST, the growth rate along the b-axis slows down significantly with respect to that of the a-axis; and (iii) when excess OA is present, the growth along the b-axis slows down but not as significantly as in the previous case. While we have shown in this paper the enhancement of the (010) face, it may also be possible to develop the (100) face by using an appropriate combination of additives which can be tried in the future.

Conclusion

Nucleation studies reveal the two step mechanism adopted by DAST molecules to grow into a single crystal. The spherulite patterns of the different compositions reveal how oleic acid reduces the cluster formation during nucleation of DAST crystals. Although several additives have been used previously, for the first time the (010) face of the DAST crystal is successfully developed by employing OA as an additive during the growth of the crystal. Apart from the morphology, the size of the crystals also increases considerably when compared to other methods reported previously. Moreover, this method is cost-effective as it reduces the quantity of DAST required to grow suitable crystal sizes for THz applications.

Acknowledgements

The authors would like to thank Dr. Mauricio Fuentealba, Laboratorio de Química Inorgánica, Instituto de Química, Pontificia Universidad Católica de Valparaíso, Valparaíso, Chile for providing single crystal XRD analysis. This work was partially supported by CONICYT-ALMA project number 31110014.

References

1. M. Tonouchi, *Nature Photon.*, 2007, **1**, 97.
2. A. Wooten and A. R. Thompson, *Proceedings of the IEEE*, 2009, **97**, 1463.
3. Don Arnone, *MIT Technology Review*, 2004, **32**, 6.
4. B. Ferguson and X. C. Zhang, *Nature Mater.*, 2002, **1**, 26.
5. P. H. Siegel, *Microwave Theory and Techniques, IEEE Transactions on*, 2002, **50**, 910.
6. C. M. Armstrong, *Spectrum, IEEE*, 2012, **49**, 36.
7. I. Wilke and S. Sengupta, *Nonlinear Optical Techniques for Terahertz Pulse Generation and Detection—Optical Rectification and Electrooptic Sampling, Terahertz Spectroscopy: Principles and Applications*, Susan L. Dexheimer (Ed), CRC Press, pp. 42, 2007.
8. M. G. Krishna, S. D. Kshirsagar and S. P. Tewari, *Terahertz Emitters, Detectors and Sensors: Current Status and Future Prospects*, Photodetectors, Dr. Sanka Gateva (Ed.), ISBN: 978-953-51-0358-5, InTech, 2012.
9. M. Jazbinsek, L. Mutter and P. Gunter, *IEEE J. Sel. Top. Quant. Electron.*, 2008, **5**, 1298.
10. X. Zheng, C. V. McLaughlin, P. Cunningham and L. M. Hayden, *Journal of Nanoelectronics and Optoelectronics*, 2007, **2**, 58.
11. K. Miyamoto, S. Ohno, M. Fujiwara, H. Minamide, H. Hashimoto and H. Ito, *Optics Express*, 2009, **17**, 14832.
12. I. Katayama, R. Akai, M. Bito, H. Shimosato, K. Miyamoto, H. Ito and M. Ashida, *Applied Physics Letters*, 2010, **97**, 021105-1.
13. M. Yusuke, T. Yoshinori, I. Takashi, Y. Masashi, Y. Yoke Khin and S. Takatomo, *Japanese Journal of Applied Physics*, 2000, **39**, L1006.
14. H. Adachi, Y. Takahashi, J. Yabuzaki, Y. Mori and T. Sasaki, *J. Cryst. Growth*, 1999, **198-199**, 568.
15. S. R. Marder, J. W. Perry and C. P. Yakymyshyn, *Chemistry of Materials*, 1994, **6**, 1137.
16. B. Ruiz, M. Jazbinsek and P. Günter, *Crystal Growth & Design*, 2008, **8**, 4173.
17. U. Meier, M. Bosch, C. Bosshard, F. Pan and P. Gunter, *Journal of Applied Physics*, 1998, **83**, 3486.
18. A. Schneider, M. Neis, M. Stillhart, B. Ruiz, R. U. A. Khan and P. Günter, *J. Opt. Soc. Am. B*, 2006, **23**, 1822.
19. F. Pan, M. S. Wong, C. Bosshard and P. Günter, *Advanced Materials*, 1996, **8**, 592.
20. Y. Namba, M. Tsukahara, A. Fushiki, K. Soizu, H. Ito, *Proceedings of SPIE*, 2003, **5180**, 55.
21. T. Kaino, B. Cai and K. Takayama, *Advanced Functional Materials*, 2002, **12**, 599.
22. F. Pan, K. McCallion and M. Chiappetta, *Applied Physics Letters*, 1999, **74**, 492.
23. A. S. Haja Hameed, W. C. Yu, C. Y. Tai and C. W. Lan, *Journal of Crystal Growth*, 2006, **292**, 510.
24. A. S. Haja Hameed, S. Rohani, W. C. Yu, C. Y. Tai and C. W. Lan, *Materials Chemistry and Physics*, 2007, **102**, 60.
25. Z. Sun, T. Chen, J. Luo and M. Hong, *Journal of Crystal Growth*, 2011, **328**, 89.
26. J. I. Wu, R. Gopalakrishnan, C. I. D. Tai and C. W. Lan, *Japanese Journal of Applied Physics, Part 1*, 2004, **43**, 1507.
27. K. Kumar, R. N. Rai and S. B. Rai, *Applied Physics B: Lasers and Optics*, 2009, **96**, 85.
28. C. Karthikeyan, A. S. Haja Hameed, J. Sagaya Agnes Nisha and G. Ravi, *Spectrochimica Acta Part A*, 2013, **115**, 667.
29. W. Bu, Z. Chen, F. Chen and J. Shi, *The Journal of Physical Chemistry C*, 2009, **113**, 12176.
30. X. Liang, L. Gao, S. Yang and J. Sun, *Advanced Materials*, 2009, **21**, 2068.
31. N. Patra, M. Salerno, A. Diaspro and A. Athanassiou, *Microelectronic Engineering*, 2011, **88**, 1849.
32. W. Kaminsky, *Journal of Applied Crystallography*, 2005, **38**, 566.
33. A. G. Shtukenberg, Y. O. Punin, E. Gunn and B. Kahr, *Chemical Reviews*, 2011, **112**, 1805.
34. L. Gránásy, T. Pusztai, G. Tegze, J. A. Warren and J. F. Douglas, *Physical Review E*, 2005, **72**, 011605.
35. A. A. Chernov, *Journal of Crystal Growth*, 1999, **196**, 524.
36. P. G. Vekilov, *Journal of Crystal Growth*, 2005, **275**, 65.
37. R. Jerald Vijay, N. Melikechi, T. Rajesh Kumar, J. G. M. Jesudurai and P. Sagayaraj, *Journal of Crystal Growth*, 2010, **312**, 420.
38. K. Jagannathan, S. Kalainathan, T. Gnanasekaran, N. Vijayan and G. Bhagavannarayana, *Crystal Growth and Design*, 2007, **7**, 859.
39. R. Jerald Vijay, N. Melikechi, Tina Thomas, R. Gunaseelan, M. Antony Arockiaraj and P. Sagayaraj, *Mater. Chem. Phys.*, 2012, **132**, 610.
40. T. Vijayakumar, I. Hubert Joe, C. P. Reghunadhan Nair, M. Jazbinsek and V. S. Jayakumar, *Journal of Raman Spectroscopy*, 2009, **40**, 52.
41. P. Tandon, G. Förster, R. Neubert and S. Wartewig, *Journal of Molecular Structure*, 2000, **524**, 201.
42. K. Nagaoka, H. Adachi, S. Brahadesewaran, T. Higo, M. Takagi, M. Yoshimura, Y. Mori and T. Sasaki, *Japanese Journal of Applied Physics*, 2004, **43**, L261.
43. T. Matsukawa, M. Yoshimura, Y. Takahashi, Y. Takemoto, K. Takeya, I. Kawayama, S. Okada, M. Tonouchi, Y. Kitaoka, Y. Mori and T. Sasaki, *Japanese Journal of Applied Physics*, 2010, **49**, 0755021.
44. A. S. Haja Hameed, W. C. Yu, Z. B. Chen, C. Y. Tai and C. W. Lan, *Journal of Crystal Growth*, 2005, **282**, 117.
45. S. Brahadesewaran, S. Onduka, M. Takagi, Y. Takahashi, H. Adachi, T. Kamimura, M. Yoshimura, Y. Mori, K. Yoshida and T. Sasaki, *Crystal Growth & Design*, 2006, **6**, 2463.
46. W. Bu, Z. Chen, F. Chen, J. Shi, *The Journal of Physical Chemistry C*, 2009, **113**, 12176.
47. C. W. Hoerr, H. J. Harwood, *The Journal of Physical Chemistry*, 1952, **56**, 1068.
48. S. Follonier, M. Fierz, I. Biaggio, U. Meier, C. Bosshard and P. Günter, *J. Opt. Soc. Am. B*, 2002, **19**, 1990.

Electronic Supplementary Information (ESI) available: Table of the sample compositions, videos of nucleation mechanism of samples A, B and C, simulated powder XRD pattern of pure and hydrated DAST, NMR and Raman spectra of pure DAST and sample B, Face indexing of sample B, Hydrogen bonding within the unit cell of DAST. See DOI: 10.1039/b000000x/

Figure captions:

Fig. 1. Measured solubility curve of DAST in methanol. Nucleation curves of samples A, B and C.

Fig. 2. Micrographs of spherulite formation in sample A (a,b), B (c,d) and C (e,f). All micrographs were taken under crossed polarization filters. Note that only sample A displays the Maltese crosses.

Fig. 3. DAST Crystals grown using OA from samples (a) A, (b) B, (c) C and (d) single crystal of sample B after separation from other crystals sticking to it.

Fig. 4. Powder XRD pattern of (a) pure DAST in powder form and (b) sample B on 001 face.

Fig. 5. (a) Simulated morphology of the DAST crystal system with the calculated interfacial angles, (b) Measured interfacial angles of the DAST crystal grown from sample B.

Fig. 6. (a) Etching of sample B with methanol, (b) magnified image of fig. a, (c) pure DAST with methanol-OA and (d) etching of a pure DAST crystal with methanol.

Fig. 7. (a) Morphology of DAST Crystals belonging to sample B, (b) Packing of DAST molecules in sample B and (c) possible interaction of OA with the (010) face of the DAST crystal.

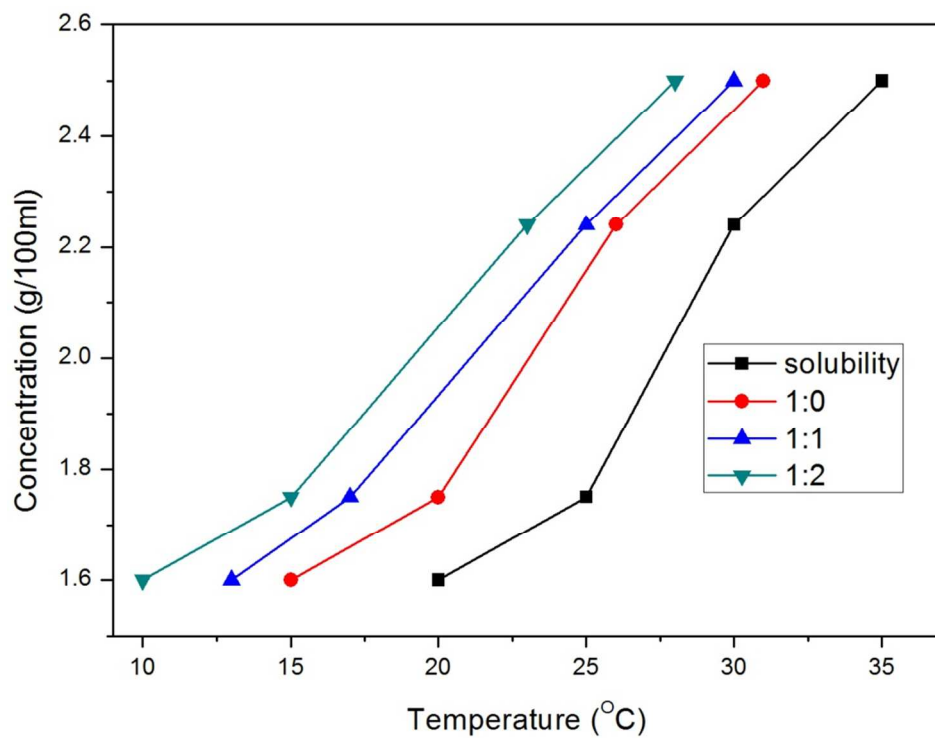


Fig. 1. Measured solubility curve of DAST in methanol. Nucleation curves of samples A, B and C.

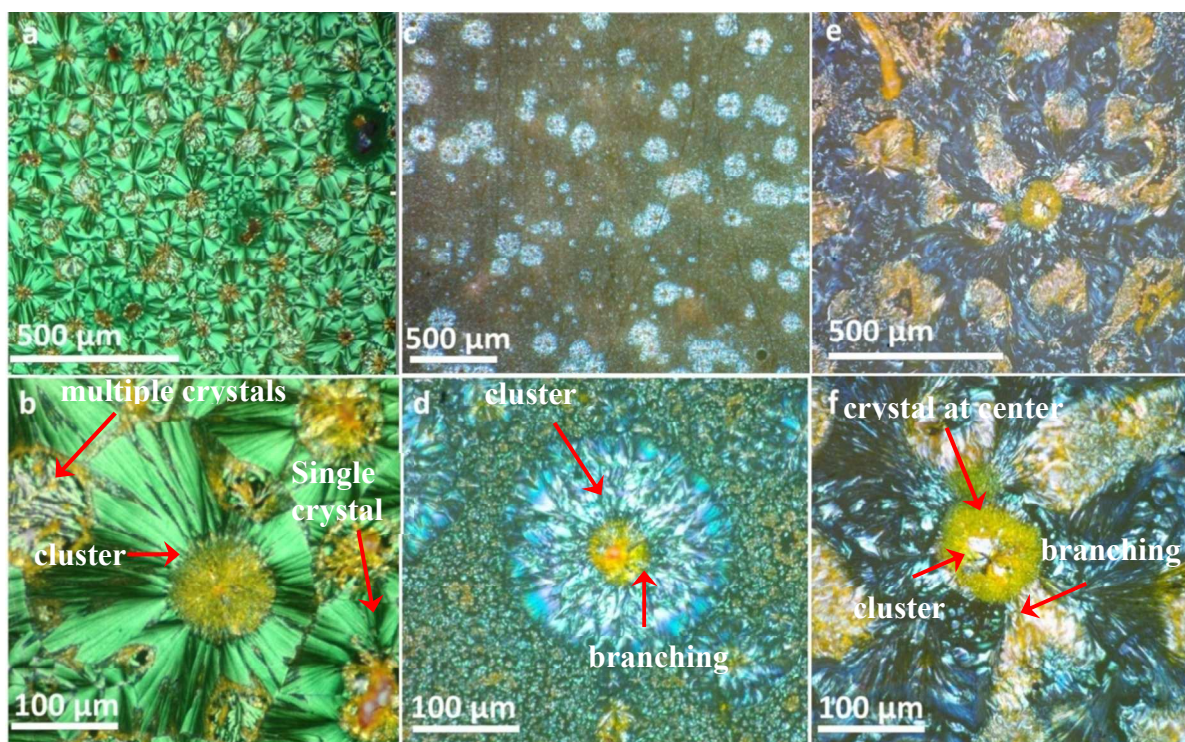


Fig. 2. Micrographs of spherulite formation in sample A (a,b), B (c,d) and C (e,f). All micrographs were taken under crossed polarization filters. Note that only sample A displays the Maltese crosses.

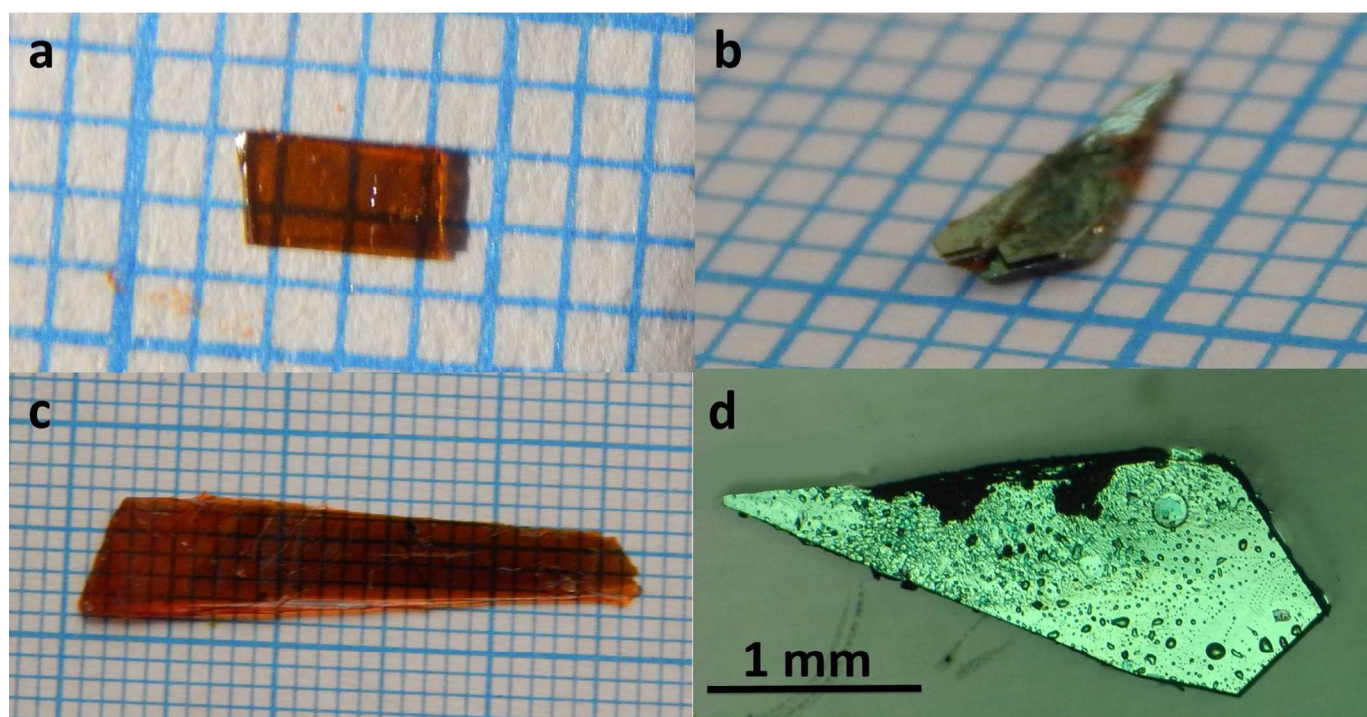


Fig. 3. DAST Crystals grown using OA from samples (a) A, (b) B, (c) C and (d) single crystal of sample B after separation from other crystals sticking to it.

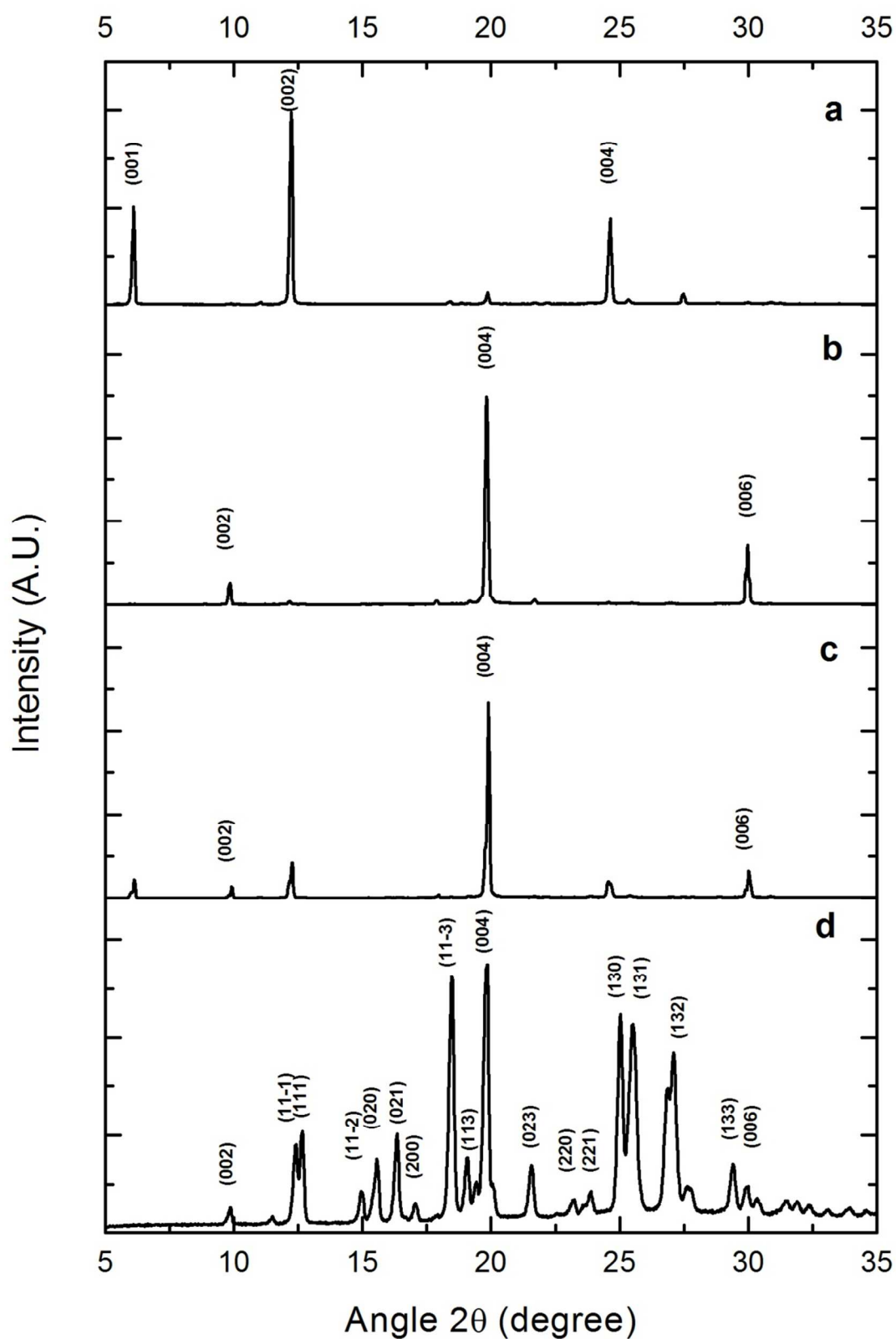


Fig. 4. Powder XRD patterns on 001 face of (a) sample A, (b) sample B, (c) sample C and (d) pure DAST in powder form.

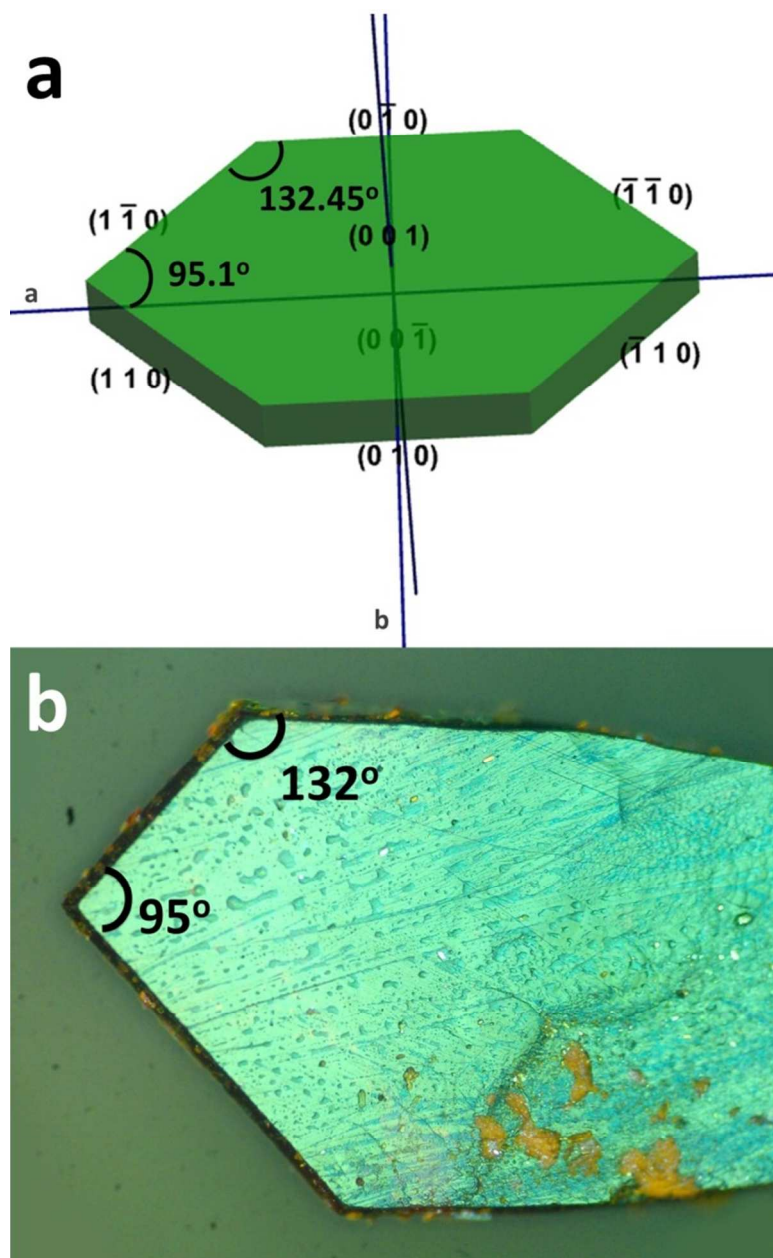


Fig. 5. (a) Simulated morphology of the DAST crystal system with the calculated interfacial angles, (b) Measured interfacial angles of the DAST crystal grown from sample B.

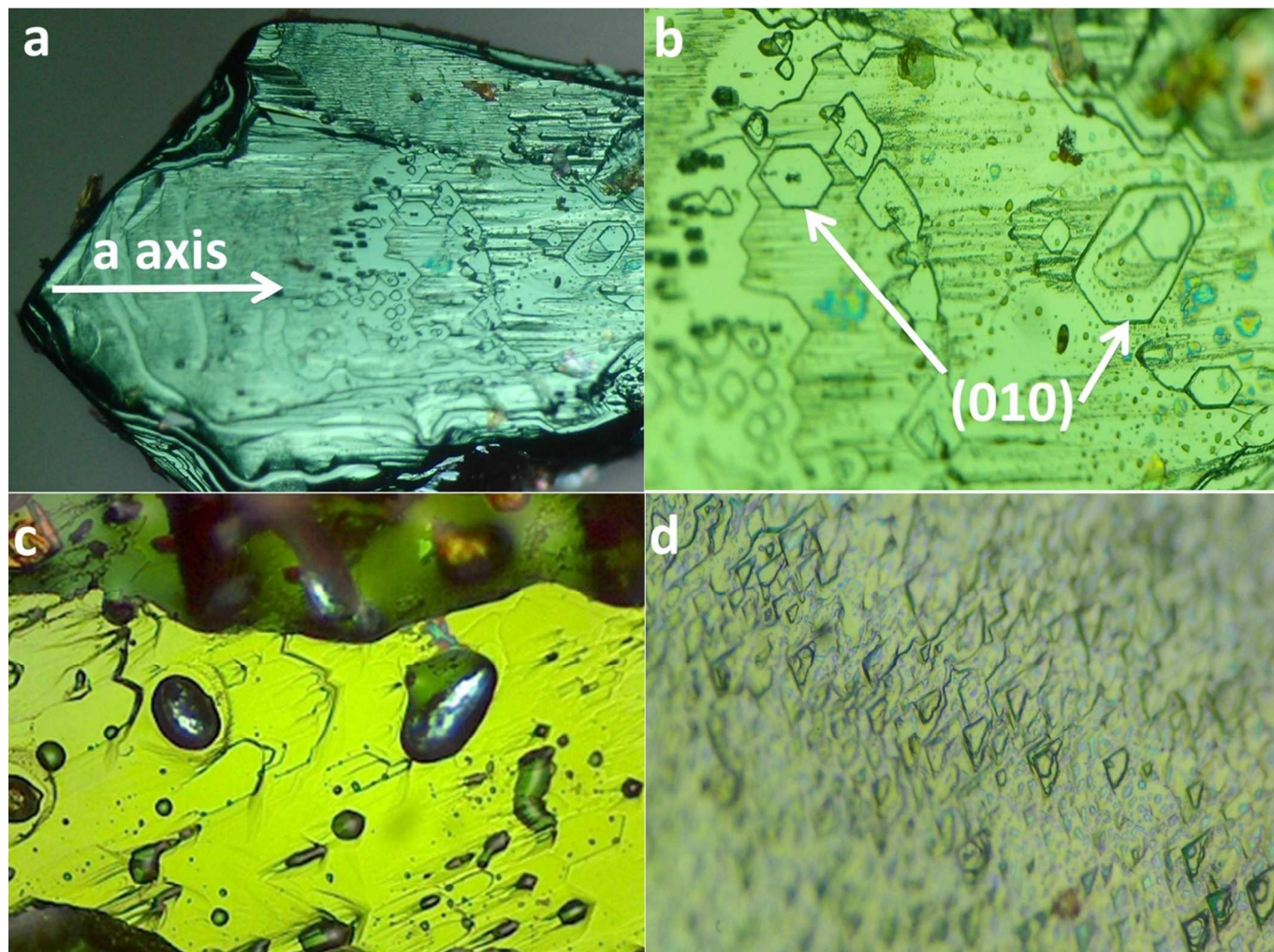


Fig. 6. (a) Etching of sample B with methanol, (b) magnified image of fig. a, (c) pure DAST with methanol-OA and (d) etching of a pure DAST crystal with methanol.

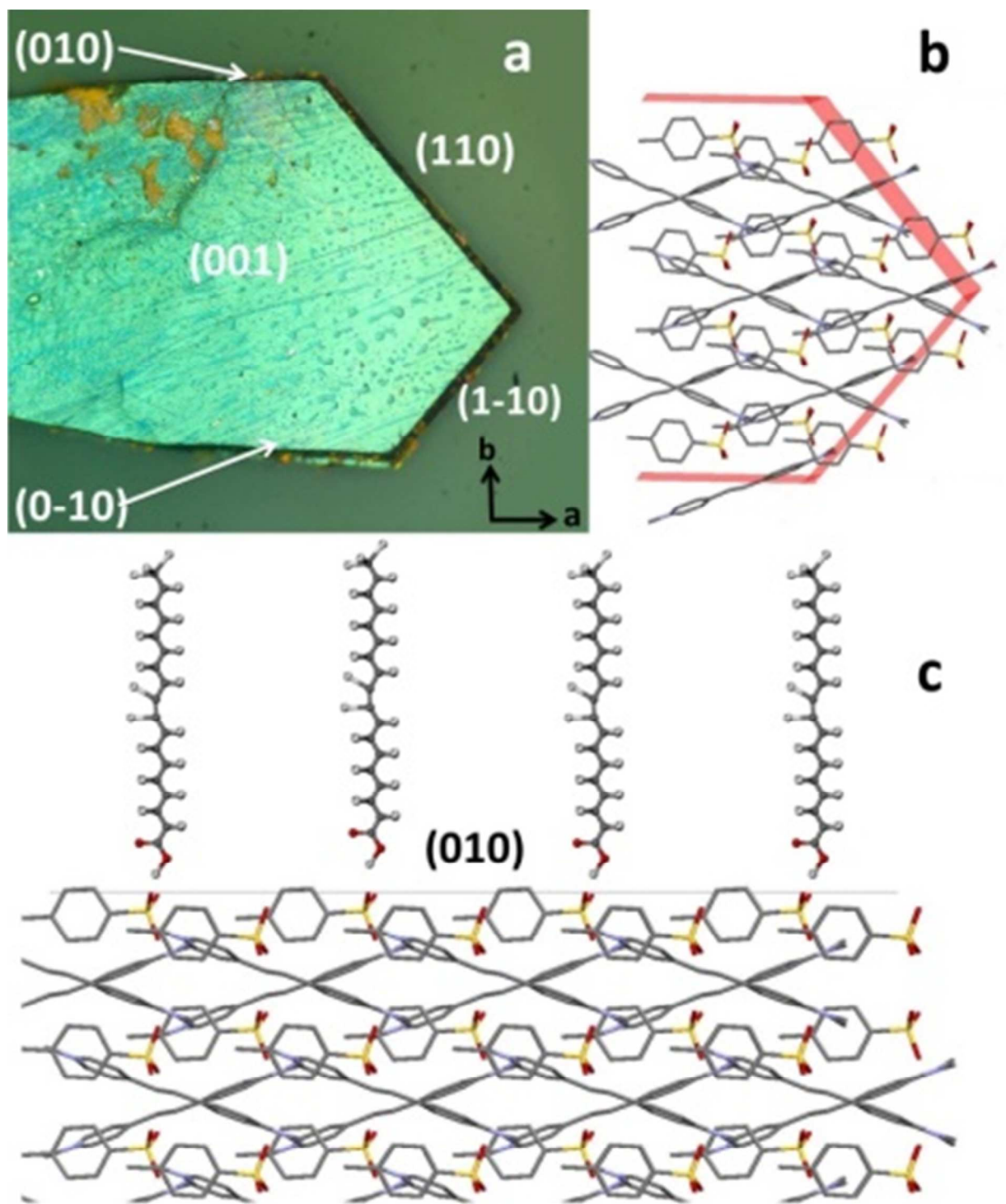
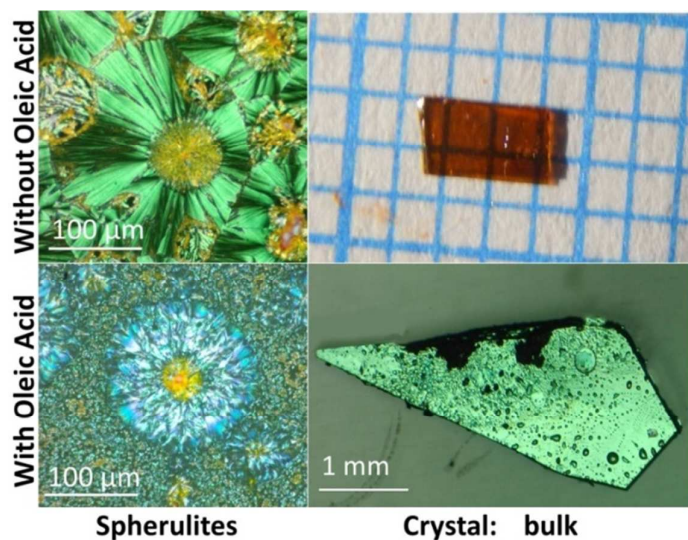


Fig. 7 (a) Morphology of DAST Crystals belonging to sample B, (b) Packing of DAST molecules in sample B and (c) possible interaction of OA with the (010) face of the DAST crystal.



A simple method to control the nucleation and morphology of (4-N, N-dimethylamino-4-N-methylstilbazoliumtosylate) DAST crystals is explored. At equal concentration of oleic acid and DAST in methanol, pure DAST crystals with an irregular hexagonal shape are obtained by solvent evaporation method. The influence of oleic acid on facilitating growth in specific faces is investigated. The purity of the grown crystal is investigated by Powder XRD, NMR and Raman spectroscopy analyses. As a major improvement we present a method where a preference in the growth of one of the desired faces (010) in the final morphology of the DAST crystal is possible which would be attractive for Terahertz generation and detection studies.